

# Influence of the number of ligands and point group on the electronic structure of $\text{Co}^{2+}$ aqua-complexes

Liesbeth De Bruecker<sup>a</sup> and prof. Veronique Van Speybroeck<sup>\*,a</sup>

October 3, 2022

<sup>a</sup> Center for Molecular Modeling(CMM), Ghent University, Technologiepark 46, 9052 Zwijnaarde, Belgium

\* Veronique Van Speybroeck E-mail: Veronique.VanSpeybroeck@UGent.be

## Abstract

The nucleation process of zeolitic imidazolate frameworks (ZIFs) is, up until now, not yet completely understood, making the search for tailored materials very difficult. Recently, it has been shown that, during the formation process, the symmetry of the precursors is reduced by ligand elimination and substitution reactions. The octahedral precursors with simple ligands, such as water, methanol, and/or  $\text{NO}_3^-$  are transformed to 5 and finally 4-coordinated complexes with imidazole ligands. This reduction of the symmetry, caused both by the changing coordination environment as well as distortions from the perfect symmetry leading to another point group, will have a large influence on the electronic structure and more specifically on the  $d$ -orbital splitting. This, on his turn, will affect the  $d - d$  electronic excitations which can be followed by using UV-Vis spectroscopy and which can help to unravel the formation process. In this work, we systematically investigate how the lowering of the number of ligands affects the symmetry and thus the geometry and electronic structure of  $\text{Co}^{2+}$  complexes with 6, 5, and 4 aqua ligands. Therefore, we first resort to qualitative techniques, such as crystal field theory (CFT) and ligand field theory (LFT), which reveal that the orbital splitting is characteristic for the number of ligands. However, as these techniques are not capable of providing quantitative results without the use of experimental data as input, we perform various computational calculations.

Both average of configuration (AOC) and unrestricted density functional Theory (UDFT) are thoroughly investigated and we will determine which technique is the best suited to properly describe the ground state of these systems. To investigate the dependency on the  $d$ -orbital occupation, we also investigated  $V^{2+}$ ,  $Mn^{2+}$ , and  $Ni^{2+}$  hexa-aqua-complexes and compared them to the Co systems.

## 1 Introduction

Zeolitic imidazolate frameworks (ZIFs) are a sub-class of metal-organic frameworks (MOFs) in which divalent metal cations, mostly  $Fe^{2+}$ ,  $Co^{2+}$ ,  $Cu^{2+}$ , or  $Zn^{2+}$ , are tetrahedrally coordinated by bridging imidazolate-type linkers<sup>1,2,3,4,5,6</sup>. Since the cation-linker-cation angle in ZIFs is similar to the Si-O-Si angle in zeolites, they are topologically isomorphic, hence their name<sup>1,7,8,9</sup>. ZIFs are due to their chemical stability, robust porosity, and resistance to thermal changes very promising candidate materials for several applications. Among others, we mention the use as catalysts or carbon dioxide caption materials<sup>10</sup>, molecular sieves for gas separation<sup>11</sup>, and high-impact shock absorbers<sup>12</sup>. Zn-ZIF-8 is a typical model system, consisting of tetrahedrally coordinated  $Zn^{2+}$  ions bridged by 2-methylimidazolate (2-mIm)<sup>1,3,5,13,14,15</sup>. By replacing the  $Zn^{2+}$  cations with  $Co^{2+}$ , the iso-structural Co-ZIF-67 is obtained<sup>16,17,18,19</sup>, which has a sodalite topology and  $Co(2-mIm)_4^{2-}$  tetrahedral secondary building units (SBUs) as shown in Figure 1.

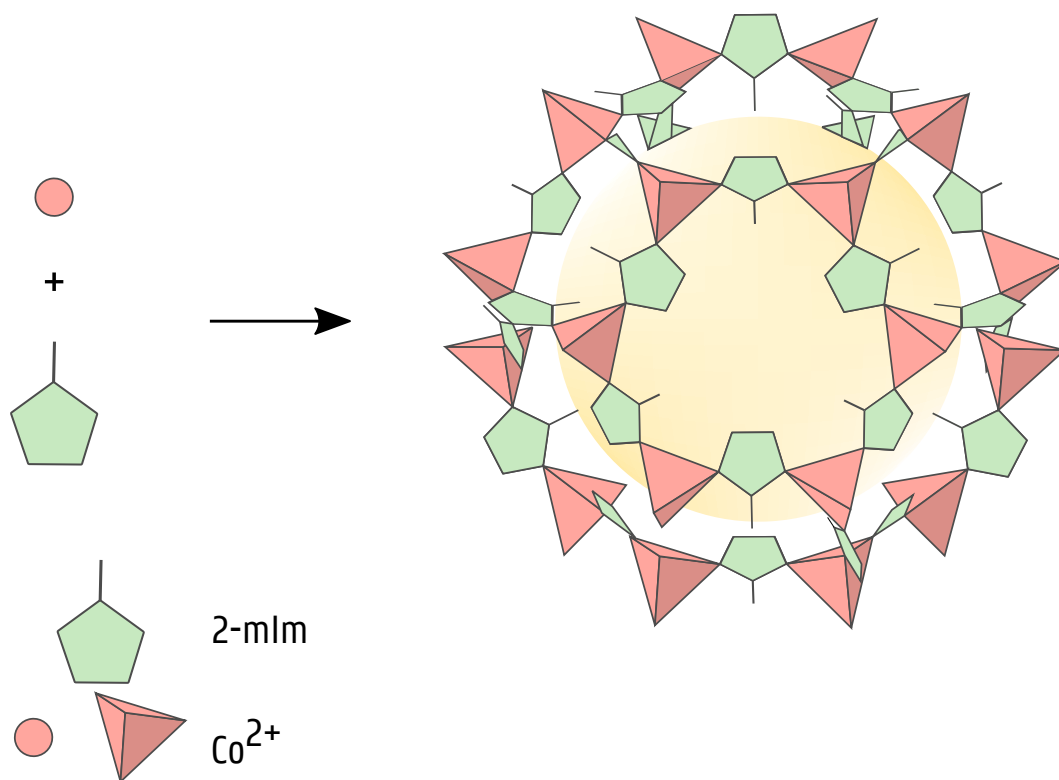


Figure 1: Crystal structure of Co-ZIF-67.  $\text{Co}^{2+}$  is indicated with a circle when it is isolated and with a tetrahedron when coordinated with the 2-mIm linkers. Figure adapted from Ref.<sup>20</sup> with permission of Elsevier, 2015.

An in-depth understanding of the formation process of these materials is indispensable for a targeted search for structures with the best properties for a specific application, as this is at the moment mainly done via high-throughput synthesis<sup>21</sup>. Although the particle nucleation step is more or less understood by now<sup>22,23</sup>, the underlying molecular assembly processes in the pre-nucleation stage have been less thoroughly investigated and remain largely unknown. Only very recently, a combined experimental-computational study has been conducted<sup>24</sup>, in which it is suggested that, during Co-ZIF-67 nucleation, a metal-organic pool with a variety of complexes is formed caused by ligand elimination and substitution reactions. This is visualized with green and blue arrows respectively in Figure 2. In this way, the symmetry of the octahedral precursors in methanol solution,  $[\text{CoL}_6]^{2+}$ , with  $L$  simple ligands like aqua, methanol, and/or  $\text{NO}_3^-$ , is lowered by 2 mechanisms during the nucleation process. On one hand, some of the ligands are substituted with imidazole, on the other hand, some of them are eliminated. The complex thus goes from  $[\text{CoL}_6]^{2+}$ , an octahedral system with 6 simple ligands, over a 5-coordinated system, towards  $\text{Co}(\text{2-mIm})_4^{2+}$ , a tetrahedral complex with 4 2-mIm ligands, which are the building blocks of Co-ZIF-67. In order to fully understand this complicated mechanism, we would like to follow the evolution of the UV-Vis spectrum, and more specifically, of the  $d-d$

transitions, as the number of them and the intensity with which they occur, change during the course of the formation process and can therefore serve as a fingerprint for the crystal formation process. An excellent recent review on computational molecular spectroscopy can be found in Ref.<sup>25</sup>.

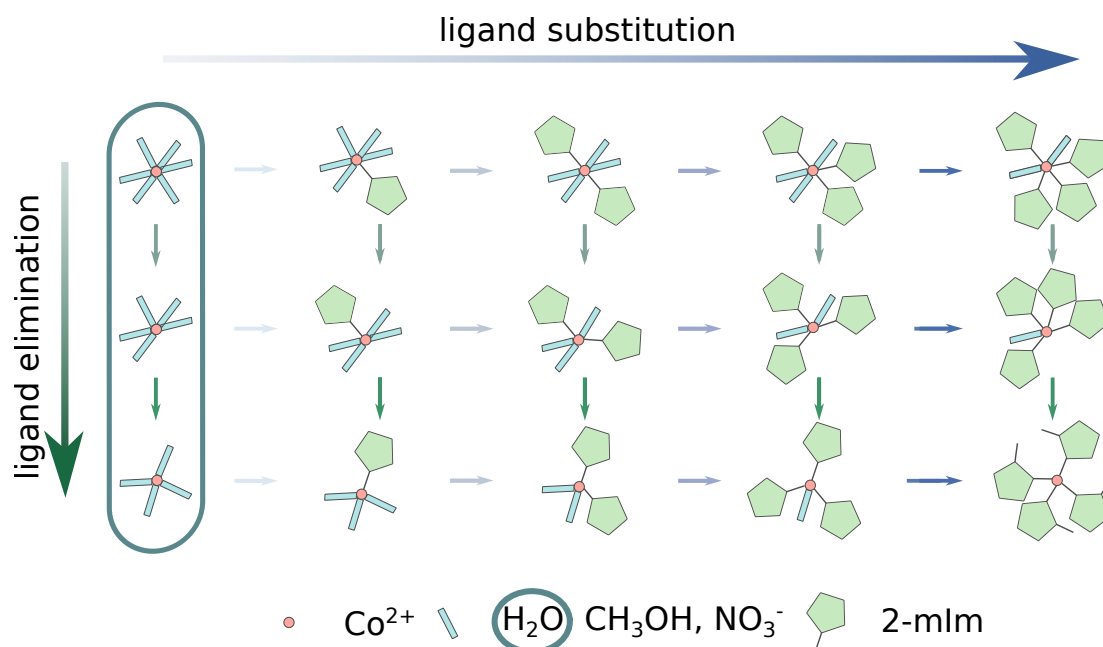


Figure 2: Reaction network of ligand elimination- and substitution reactions leading to fast pre-equilibrium formation toward a metal-organic pool.  $\text{Co}^{2+}$  complexes with 6, 5, and 4 aqua ligands are studied in this work and are indicated. Figure adapted from Ref.<sup>24</sup> with permission of Elsevier, 2021.

In this work, we investigate 6-coordinated octahedral, 5-coordinated square pyramidal (SP), 5-coordinated trigonal bipyramidal (TBP), and 4-coordinated tetrahedral  $\text{Co}^{2+}$  complexes, as shown in Figure 2. We restrict ourselves to aqua ligands as, in particular for hexa-aqua  $\text{Co}^{2+}$  complexes, we can compare our results to previous studies. We will concentrate on the ground state properties as they need to be described correctly and understood completely before an investigation of the excited states can be started. The ground state properties of TMCs still pose various challenges as for example recently shown in Ref.<sup>26</sup> and in Ref.<sup>27</sup> for the calculation of spin state energetics.

As stated before, octahedral  $\text{Co}^{2+}$  aqua-complexes have already been extensively studied in literature. Structural properties and excitation energies have been obtained from experimental studies<sup>28,29,30,31,32,33</sup>. Besides this,  $[\text{Co}(\text{H}_2\text{O})_6]^{2+}$  has also been the subject of many computational investigations as it can serve as a model system for much more complicated  $\text{Co}^{2+}$  complexes, and, due to its small size, direct comparisons to highly correlated *ab initio* calculations

are feasible<sup>34</sup>. A detailed review of the ground state properties using a wide variety of computational methods has been given in Ref.<sup>35</sup>. More recent works also investigate the excited states, but this lies outside the scope of this work<sup>36,37,38,39</sup>. These complexes have also already been investigated using multireference ab initio calculations where solvent effects have been included<sup>40</sup>.

In the present study, we will extend the computational results by examining the electronic structure of these complexes, and more specifically, we will focus on the influence of symmetry on the position of the energy levels of the  $d$ -orbitals as this is decisive for the  $d-d$  transitions. There are two origins for the changes in symmetry. First of all, large influences are expected when the number of ligands is changed, resulting in various coordination environments, *i.e.*, octahedral, SP, TBP, and tetrahedral. Furthermore, additional effects will be studied for the various point groups encountered for each coordination environment as we will notice that deviations from the perfect symmetry are present. We will search for, and find, stable structures which are capable of reproducing the experimental data. Furthermore, we will explore how the properties of these complexes change when 1 and 2 of the aqua-ligands are removed and how this reduction in symmetry is translated in alternations of the  $d$ -orbital splitting. In order to validate our results, we will make comparisons with experimental data where possible.

The remainder of this work is organized as follows. First, we focus on the qualitative predictions for the  $d$ -orbital splitting in various coordination symmetries obtained from theoretical techniques such as crystal field theory (CFT), Ligand field theory (LFT), and the angular overlap method (AOM). In the next section, the results from DFT calculations, both average of configuration (AOC) and unrestricted density functional Theory (UDFT), are discussed. The molecular orbitals (MOs) with large contributions from  $d$ -orbitals will be studied in-depth and more particular, we will concentrate on the influence of symmetry on the splitting of these orbitals. We will determine which technique is suited to correctly describe the ground-state properties of these transition metal complexes (TMCs). Besides  $\text{Co}^{2+}$ , we will also investigate other transition metals,  $\text{V}^{2+}$ ,  $\text{Mn}^{2+}$ , and  $\text{Ni}^{2+}$ , of which the  $d$ -orbital splitting poses less challenges, as will be explained in Section 3.6. In the final section, we conclude with the main outcomes obtained in this study. An overview of the systems studied in this work is given in Table 1.

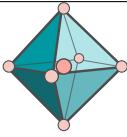
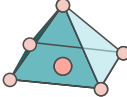
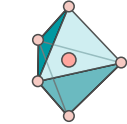
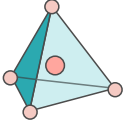
Number of aqua ligands	Symmetry	Visualisation of geometry	Elements studied
6	Octahedral		$\text{Co}^{2+}$ , $\text{V}^{2+}$ , $\text{Mn}^{2+}$ , $\text{Ni}^{2+}$
5	Square pyramidal (SP)		$\text{Co}^{2+}$
	Trigonal bipyramidal (TBP)		$\text{Co}^{2+}$
4	Tetrahedral		$\text{Co}^{2+}$

Table 1: Overview of the complexes studied in this work, ordered based on their number of aqua ligands. For every system, both AOC and UDFT calculations are performed. Experimental data are available for the 6-coordinated complexes.

## 2 Qualitative insights into the $d$ -orbital splitting via CFT, LFT and AOM

In the past century, several theoretical models have been introduced to describe the electronic structure of TMCs, which are still extensively used. First, Becke and Von Vleck applied the CFT, which already existed for the description of metal ions in crystals, to isolated TMCs<sup>41,42,43</sup>. In this electrostatic approach, ligands are approximated by point charges. The metal  $d$ -orbitals pointing towards the ligands will raise in energy due to electrostatic repulsion, whereas the  $d$ -orbitals directed between the ligands remain relatively unaffected. As such, this approach predicts the  $d$ -orbital splittings in coordination complexes with various symmetries. However, as this method does not describe metal-ligand bonding, LFT, combining CFT and molecular orbital theory (MOT), has been introduced by Griffith and Orgel<sup>44</sup>. It describes the interactions between metal and ligand frontier orbitals which are responsible for the formation of MOs. Additionally, the AOM takes into account the angular geometry of the complex and estimates the strength of interaction between individual ligand orbitals and metal  $d$ -orbitals based on their mutual overlap<sup>45,46</sup>. The benefit of this technique is that it is capable of treating systems with little or no symmetry. This comes at the cost of the large number of parameters to be de-

terminated from experiment<sup>47</sup>. These models present different approaches to solve the electronic structure of TMCs and all have their advantages and disadvantages, but in general, they give the same qualitative results. These methods can be made quantitative by determining the parameters from experimental absorption spectra. However, we will not focus on this and only give a qualitative explanation of the results as shown in Figure 3 for complexes with various symmetries.

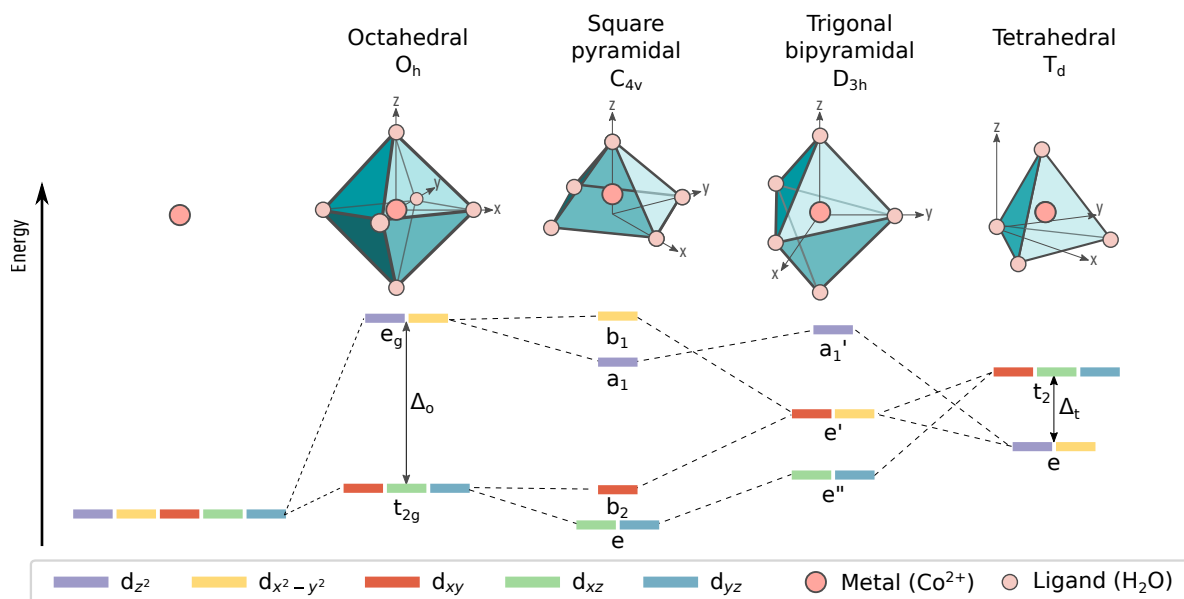


Figure 3: Splitting of the  $d$ -orbitals for a TM in various environments. For an isolated TM, all  $d$ -orbitals are degenerate, whereas for complexes with octahedral, SP, TBP, and tetrahedral symmetry, the degeneracy is (partially) lifted. The splitting between the two orbital sets in octahedral and tetrahedral complexes is denoted by  $\Delta_o$  and  $\Delta_t$  respectively. The labeling of the  $d$ -orbitals in the various point groups is also indicated.

For an isolated TM ion, all 5  $d$ -orbitals are degenerate, *i.e.*,  $d_{z^2}$ ,  $d_{x^2-y^2}$ ,  $d_{xy}$ ,  $d_{xz}$ , and  $d_{yz}$ , indicated in purple, yellow, red, green, and blue respectively, and have the same energy. A graphical visualization of these orbitals is shown in Figure 4. Two of them, *i.e.*,  $d_{z^2}$  and  $d_{x^2-y^2}$ , have lobes which are oriented along the coordinate axes, whereas the lobes of the other orbitals are situated in between the coordinate axes. As will be discussed later, the orientation plays an important role when coordinating with ligands. When the TM atom is surrounded by ligands, the average energy of the 5  $d$ -orbitals is above that of the free ion orbitals, because of the electrostatic field generated by the ligands. Furthermore, the degeneracy of the  $d$ -orbitals is (partially) lifted. This will be studied in the subsequent paragraphs for 6-, 5, and 4-coordinated complexes.

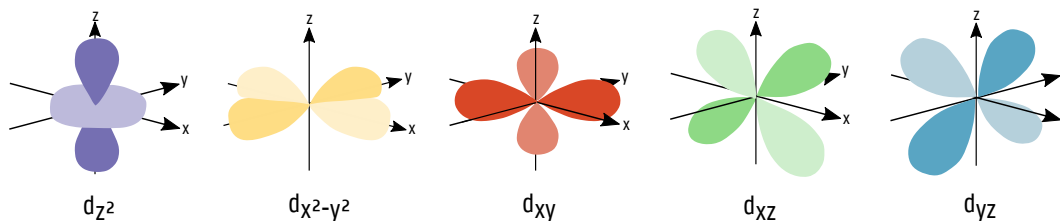


Figure 4: Graphical visualization of the 5  $d$ -orbitals:  $d_{z^2}$ ,  $d_{x^2-y^2}$ ,  $d_{xy}$ ,  $d_{xz}$ , and  $d_{yz}$ .

Octahedral complexes have 6 ligands positioned along the coordinate axes and situated at the corners of an octahedron with the TM in the center as shown in Figure 3. The degeneracy of the  $d$ -orbitals is raised partially as they split in 2 degenerate orbital sets:  $t_{2g}$  and  $e_g$ .  $d_{z^2}$  and  $d_{x^2-y^2}$  with lobes directed towards the ligands are raised in energy by the electrostatic repulsion between the electrons of the TM and the ligands and form the  $e_g$  set. The  $t_{2g}$  set contains  $d_{xy}$ ,  $d_{xz}$ , and  $d_{yz}$ , with lobes oriented in between the ligands and therefore, they remain relatively unaffected. The energy gap between these 2 sets is indicated in Figure 3 by  $\Delta_o$ , where the subscript  $o$  denotes that this is the splitting for octahedral complexes. When we assume that the ligands are spherical symmetric, the corresponding symmetry is octahedral,  $O_h$ . However, as will be seen later, the symmetry will be lowered for aqua ligands.

When removing one ligand, a distinction needs to be made between the removal of a ligand oriented along the  $z$ -direction or one lying in the  $xy$ -plane. When one of the ligands along the  $z$ -direction is eliminated, the SP structure, which belongs to the  $C_{4v}$  point group, is obtained.  $d_{z^2}$ ,  $d_{xz}$ , and  $d_{yz}$  are stabilized, compared to the octahedral case as the repulsive interaction between the orbitals and one of the ligands on the  $z$ -axis is now no longer present. When one of the ligands in the  $xy$ -plane is removed, the TBP structure, belonging to  $D_{3h}$ , is retrieved. Compared to the octahedral complex,  $d_{xy}$  and  $d_{x^2-y^2}$  are increased/decreased in energy respectively because they point more/less towards the ligands. The application of the AOM shows that the overall splitting of the  $d$ -orbitals is smaller in  $D_{3h}$  than in  $C_{4v}$  symmetry<sup>48</sup>. The labeling of the orbital sets in these point groups is indicated in Figure 3.

When, starting from the TBP structure, another ligand is taken out along the  $z$ -axis, we obtain a tetrahedral structure with  $T_d$  symmetry, in which the ligands are situated in between the coordinate axes and at the origin. In contrast to the octahedral complex,  $d_{xy}$ ,  $d_{xz}$ , and  $d_{yz}$ , grouped in  $t_2$ , now point towards the ligands, whereas  $d_{x^2-y^2}$ , and  $d_{z^2}$ , forming the  $e$  set, are situated in between the ligands. Therefore, the  $e$  set is more stable compared to the  $t_2$  set. In

a similar way as for the octahedral complexes, we can define  $\Delta_t$ , the splitting between the  $t_{2g}$  and  $e_g$  orbitals.  $\Delta_t$  is smaller compared to the octahedral case, since the ligands are not oriented directly towards the d-orbitals and therefore the effects will be smaller. This is in agreement with AOM calculations, which show that  $\Delta_t \approx \frac{4}{9}\Delta_o$ <sup>49</sup>.

These  $d$ -orbital splittings are in accordance with the LFT results of Solomon *et al.*<sup>50</sup>, who studied 6-, 5-, and 4-coordinated  $\text{Fe}^{2+}$ -complexes with oxygen-type ligands.

As stated before, quantitative  $d$ -orbital splittings can be obtained from techniques such as LFT by using experimental input data. However herein, we will perform computational calculations based on DFT in order to acquire quantitative  $d$ -orbital splittings for  $\text{Co}^{2+}$  aqua-complexes, as will be discussed in Section 3. As a consequence, we will perform computational calculations in order to obtain qualitative results for  $\text{Co}^{2+}$  aqua-complexes, as will be discussed in Section 3. These *ab initio* results can then be compared to the theoretical predictions shown in Figure 3 and to the available experimental information.

### 3 Quantitative *Ab initio* calculations: AOC and UDFT

In this section, the computational techniques used to study  $\text{Co}^{2+}$ -complexes with 6, 5, and 4 aqua ligands are explained. The results are analysed and compared to the qualitative outcomes shown in Figure 3. Before diving into this, attention is paid to the different spin multiplicities  $\text{Co}^{2+}$ -ions can possess.

The  $\text{Co}^{2+}$ -ion has 7  $d$ -electrons which can be placed in 5  $d$ -orbitals. There are 2 possible spin multiplicities, 4 and 2, forming the high spin (HS) and low spin (LS) configuration respectively. In the former, as much as possible electrons are unpaired, whereas in the latter, only 1 unpaired electron is present. According to the spectrochemical series, water is a weak ligand<sup>51</sup>. Therefore,  $\Delta_o$  in octahedral complexes is rather small and the energy needed to pair 2 electrons is larger than the energy required to place an electron in the higher-lying  $e_g$  set. Hence, the HS state of  $[\text{Co}(\text{H}_2\text{O})_6]^{2+}$  is more stable, resulting in 5  $\alpha$ - and 2  $\beta$ -electrons. This is also in agreement with the DFT study on relative stabilities reported in Ref.<sup>52</sup>. Moreover, since  $\Delta_t < \Delta_o$ , we can conclude that the HS configuration of the tetrahedral complex will also be more stable than the LS state. Finally, it has also been observed that, in 5-coordinated complexes, ligands with

oxygen donor atoms usually result in HS configurations<sup>53,54</sup>.

In this work, 2 types of calculations have been performed, AOC and UDFT, both based on DFT. In AOC, a spin-restricted self consistent field (SCF) DFT calculation of the  $d^7$  configuration is performed, in which the  $d$ -electrons are distributed evenly among the 5 MOs dominated by  $d$ -orbitals. This results in an average occupation of 1.4 electrons. One thus allows systems with fractional occupation numbers. Indeed, one of the great advantages of DFT is, as it is based on the electron density, that there is no formal constraint that orbitals must have integer occupations<sup>55</sup>. Remark that the spin multiplicity is not imposed in these calculations. Meanwhile, in UDFT, the spin multiplicity is specified and all of the 5  $\alpha$ -orbitals are filled, whereas only 2  $\beta$ -orbitals are occupied.

In the following, the AOC results are discussed in detail for  $[\text{Co}(\text{H}_2\text{O})_6]^{2+}$ ,  $[\text{Co}(\text{H}_2\text{O})_5]^{2+}$ , and  $[\text{Co}(\text{H}_2\text{O})_4]^{2+}$ . We systematically investigate how the lowering of the number of ligands affects the symmetry and thus the geometry and electronic structure of these  $\text{Co}^{2+}$ -complexes. This is followed by a comparison between AOC and UDFT. As outlined in the computational section, optimised structures have been obtained using UDFT.

### 3.1 Computational Details

The calculations, both AOC and UDFT, were performed with the Amsterdam modeling suite (AMS)<sup>56</sup>. The TZ2P+ basis set, with extra  $d$ -Slater type orbitals (STO), has been applied for the transition metals and the TZ2P basis set has been used for the other elements. Methanol has been included as a solvent using COSMO<sup>57</sup>. Radon *et al.* recently revealed that the inclusion of the second solvation shell is important to properly determine the excited states of octahedral aqua-complexes<sup>40</sup>. However, for the aqua-complexes studied in this work, the environment is more complex and consists of both water and methanol to mimic the experimental conditions valid in the formation of ZIFs. A full study of the influence of the complex solvation environment on the chemical and electronic properties of the aqua-complexes is beyond the scope of the manuscript, since here we focus on the influence of reducing the number of aqua ligands directly coordinated to the transition metal. Scalar relativistic effects were taken into account using the ZORA formalism<sup>58,59,60</sup>. Grimme D3 dispersion corrections, which affect the geometry but not the orbital energies, have also been added<sup>61</sup>. We have made use of several func-

tionals coming from different rungs on Jacob’s ladder in order to test their performance in reproducing the  $d$ -orbital splitting of  $[\text{Co}(\text{H}_2\text{O})_6]^{2+}$  with  $D_{2h}$  symmetry, which will be explained in Section 3.2, by using AOC calculations. We assessed the following functionals: BLYP<sup>62</sup> and BP86<sup>63</sup> based on the generalized gradient approximation (GGA), M06L<sup>64</sup> and MN15L<sup>65</sup> built on the meta GGA (mGGA), O3LYP<sup>66</sup>, B3LYP<sup>67,62</sup>, X3LYP<sup>68</sup>, PBE0<sup>69</sup>, and MN15<sup>70</sup> as hybrid GGA, with 12, 20, 21.8, 25 and 44 % of Hartree-Fock exchange, the hybrid mGGA TPSSh<sup>71,72</sup> with 10% Hartree-Fock exchange, and the long-range corrected CAM-B3LYP<sup>73</sup> and  $\omega$ B97x<sup>74</sup>. The results are shown in Figure 5. It stands immediately out that not enough Hartree-Fock exchange is included in O3LYP, for which the splitting between the  $e_g$  and  $t_{2g}$  set is too large. All other functionals have similar results. We have chosen to continue with B3LYP-D3.

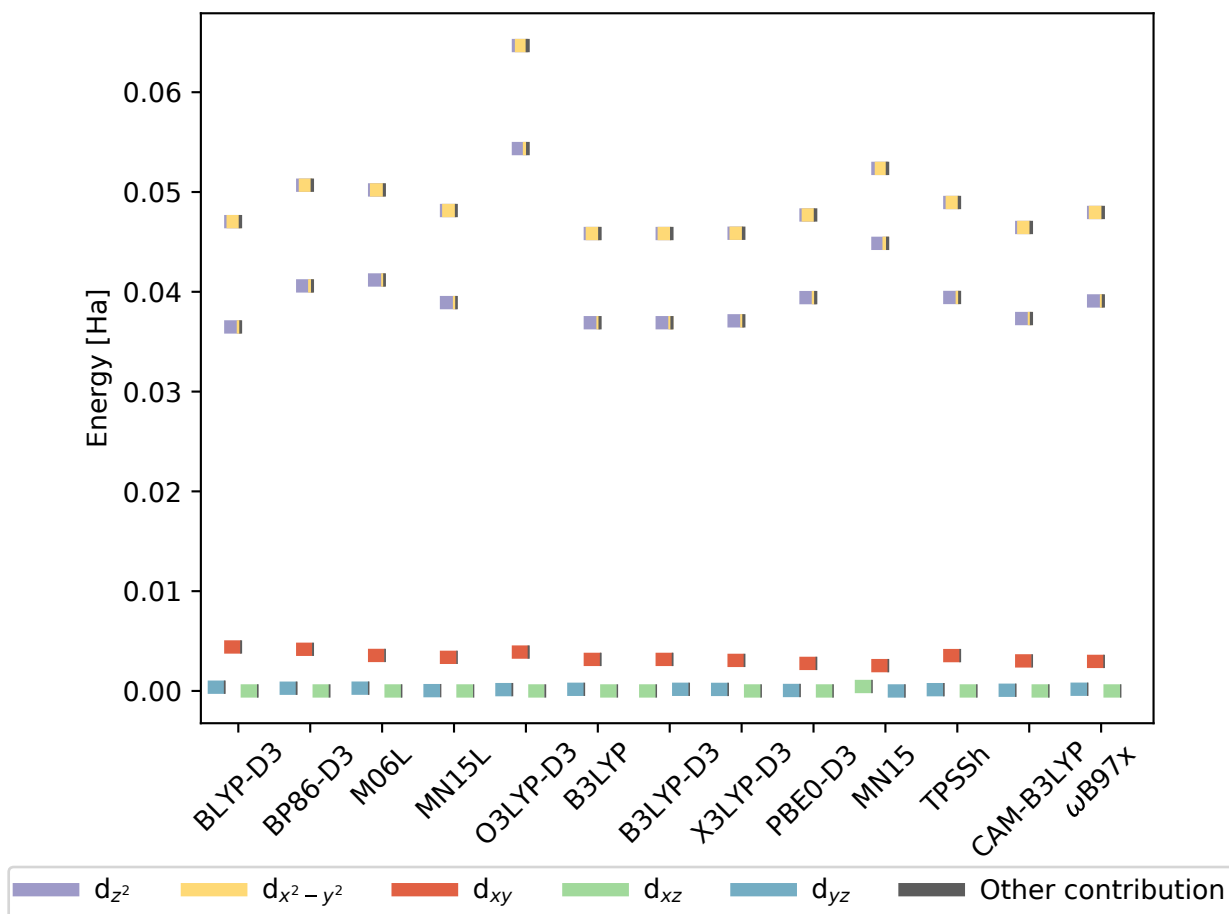


Figure 5: Splitting of the  $d$ -orbitals along with their atomic contributions for  $[\text{Co}(\text{H}_2\text{O})_6]^{2+}$  with  $D_{2h}$  symmetry obtained from AOC calculations using different functionals. Energies are shifted with respect to the lowest  $d$ -orbital.

Geometry optimisations have been performed using UDFT. We checked that all computed internal normal modes of the optimised structures show positive frequencies, ensuring that the geometries represent minima of the ground state potential energy surface. The optimised coordinates of all complexes studied in this work are shown in Table S6. The spin contamination

is negligible for all systems as shown in Table S1. The symmetry of the complexes has been determined by GaussView 5.0<sup>75</sup>.

Using the single-reference UDFT method for these challenging electronic structure systems, may at first instance appear to be unsatisfactory. However, Shee *et al.* have recently put forward that in most transition metal complexes, static correlation is rarely found in the ground states of mono-TMCs<sup>76</sup>. Furthermore, it has been shown that often good structures and energies are obtained from DFT calculations at a moderate computational cost<sup>77</sup>. Hence, we chose DFT to describe the ground state properties of these systems. Nevertheless, as there are complex interactions present, including ligand-to-metal  $\sigma$ -donation and metal-to-ligand  $\pi$ -backdonation, a proper treatment of the dynamic correlation becomes extremely important.

### 3.2 AOC: $[\text{Co}(\text{H}_2\text{O})_6]^{2+}$

Octahedral TMCs belong to the  $O_h$  point group when the ligands have spherical symmetry. However, when we take into account the structure of the aqua ligands, the highest possible symmetry becomes  $T_h$ , with 6 equivalent ligand bond distances and all O-Co-O angles equal to  $90^\circ$  or  $180^\circ$ . A graphical visualization of the symmetry elements present in the point groups encountered for  $[\text{Co}(\text{H}_2\text{O})_6]^{2+}$  is presented in Figure 6. The geometrical structure of  $[\text{Co}(\text{H}_2\text{O})_6]^{2+}$  has already been investigated thoroughly in literature. DFT studies have been performed by both Varadwaj *et al.*<sup>35</sup> and Schmiedekamp *et al.*<sup>52</sup>. Calculations have been performed at the following levels of theory respectively: UX3LYP and UB3LYP with a 6-311++G\*\* full core basis set and B3LYP with LACVP\*\* effective core potential basis set for Co and 6-31G\*\* basis for all other atoms. Varadwaj *et al.* compared their results with 163 structures containing the  $[\text{Co}(\text{H}_2\text{O})_6]^{2+}$  ion found in the Cambridge structural database (CSD)<sup>78</sup>. Most of the structures, 122 out of the 163 found in the CSD, have 3 different pairs of bond lengths, the shortest, intermediate, and longest bonds are  $2.06 \pm 0.02$ ,  $2.09 \pm 0.02$ , and  $2.11 \pm 0.02$  Å respectively. Overall, a mean Co-O bond length of  $2.09 \pm 0.03$  Å is found, with the shortest and longest value equal to 1.975 and 2.204 Å respectively. Based on the computational results of Varadwaj<sup>35</sup> and Schmiedekamp<sup>52</sup> three main conclusions can be made. First, the calculations overestimate the Co-O bond lengths by  $0.04$  Å<sup>35</sup> and  $0.06$  Å<sup>52</sup> respectively. Second, unless the geometry is specifically constrained, the distortions in the Co-O bond lengths present in most crystallographically determined structures, are not reproduced. Varadwaj *et al.* have observed a structure with distorted bond

lengths, however it is a fourth order saddle point. Third, the structure is slightly tilted. This effect is also observed in the solid state structures: 74 % of the structures found in the CSD have complementary angles that differ by more than  $4^\circ$  and nearly 12% have complementary angles differing by more than  $10^\circ$ . Note that Varadwaj<sup>35</sup> performed gas-phase calculations whereas Schmiedekamp<sup>52</sup> also studied the influence of water as a solvent.

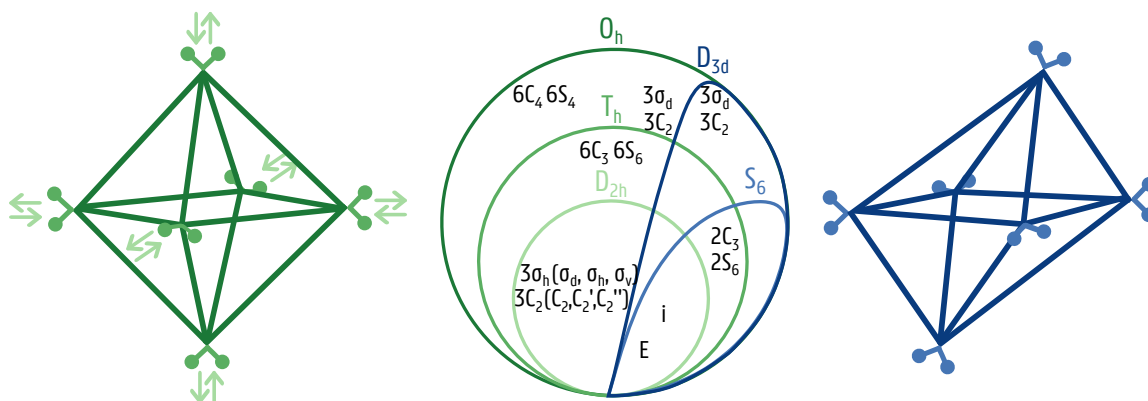


Figure 6: Graphical visualisation of the point groups encountered for the 6-coordinated complexes, *i.e.*,  $O_h$ ,  $T_h$ ,  $D_{2h}$ ,  $D_{3d}$ , and  $S_6$ . In the middle pane, all symmetry elements enclosed belong to the corresponding point group. Perfect octahedral symmetry,  $O_h$  is indicated in dark green. The presence of hydrogen atoms reduces the symmetry to  $T_h$  and is indicated in middle green. Elongation or contraction of the metal-ligand bonds results in  $D_{2h}$  symmetry and is shown in light green. An increase or decrease of the ligand-metal-ligand angles leads to a tilted structure with  $D_{3d}$  symmetry and is presented in dark blue. When the hydrogen atoms are taken into account in the tilted structure, the  $S_6$  symmetry is obtained as shown in light blue.

In contrast to the results of Varadwaj and Schmiedekamp, we did not find a stable minimum near to  $T_h$  symmetry as negative vibrational frequencies were observed. This is in agreement with the Jahn-Teller (JT) effect, which states that non-linear molecules with a spatially degenerate electronic ground state undergo a geometrical distortion in order to lower the energy of the system<sup>79</sup>. Despite the fact that only weak JT effects are expected since the  $t_{2g}$  orbitals are unevenly occupied, we observed them in the geometry optimisations. We could identify an optimised structure with  $D_{2h}$  symmetry, in which the experimentally observed JT distorted bond lengths are clearly retrieved. The observed bond lengths of the complex with  $D_{2h}$  symmetry are 2.03, 2.10, and 2.13 Å. The resulting geometric structure along with the  $d$ -orbital splitting and atomic contributions is shown in the right pane of Figure 7. This deformed structure is obtained via a rhombic distortion, *i.e.*, an unequal amount of elongation or compression along a 4-fold axis of rotation. As such, the structure remains orthogonal but the bond distances are no longer equal. Such JT distorted  $[\text{Co}(\text{H}_2\text{O})_6]^{2+}$  complexes have already been observed by Vlahovic *et al.*<sup>39</sup>. Following the methodology of Zlatar *et al.*, we calculated the JT paramete-

ters<sup>80,81</sup>. The results are shown in Table S2. Besides this, we also discovered a structure with  $S_6$  symmetry, acquired via a trigonal distortion of the complex, *i.e.*, an elongation/compression along one of the 4 3-fold symmetry axes. All ligand bond distances are equal, but the structure is no longer orthogonal. Such distorted complexes have  $D_{3d}$  symmetry when the hydrogen atoms are not taken into account. For the complex with  $S_6$  symmetry, all bond lengths are 2.10 Å and the system is tilted with 3.8°. This is shown in the left pane of Figure 7. This complex is slightly more stable than the complex with  $D_{2h}$  symmetry (-10328 kJ/mol compared to -10311 kJ/mol). The observed point groups along with their symmetry elements are displayed in Figure 6. The coexistence of two different distorted octahedral complexes has already been observed in  $K_3[MnF_6]$ <sup>82</sup>.

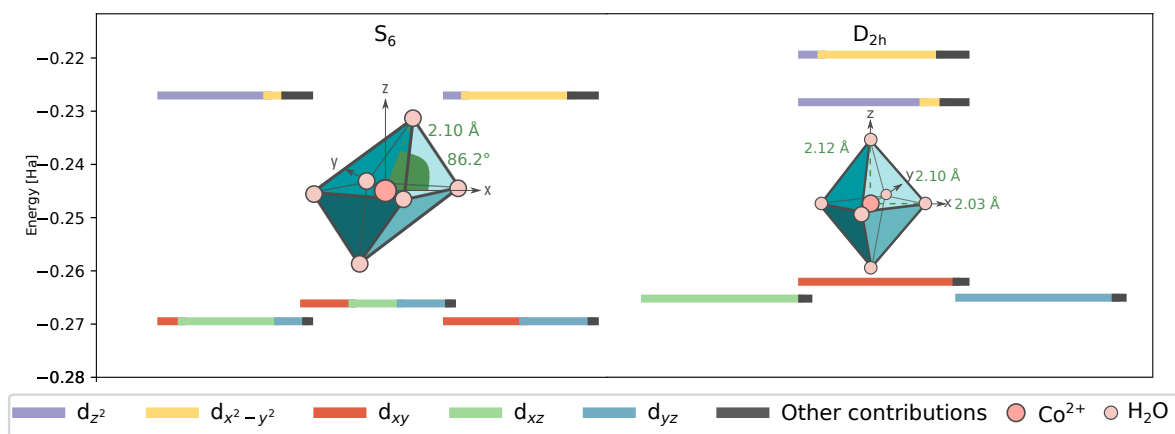


Figure 7: Splitting of the  $d$ -orbitals along with their atomic contributions for the optimised  $[Co(H_2O)_6]^{2+}$  complexes with  $S_6$  (left pane) and  $D_{2h}$  (right pane) symmetry. Some bond lengths [Å] and bond angles [°] are also indicated.

The splitting of the  $d$ -orbitals is very similar to the theoretical predictions shown in Figure 3. Some mixing with other contributions different from  $d$ -orbitals occurs, which is indicated with dark grey. In general, each MO has a dominant contribution from a specific  $d$ -orbital. This can then be used to label the MOs. This is especially the case for the complex with  $D_{2h}$  symmetry. The resulting orbitals are shown in Figure S1 and closely resemble these in Figure 4. However, there is more mixing within the  $t_{2g}$  and  $e_g$  set for the  $S_6$  complex, for which the orbitals are shown in Figure S2. For example, the highest lying  $t_{2g}$  orbital, which contains equal contributions from  $d_{xy}$ ,  $d_{xz}$ , and  $d_{yz}$ , differs from the orbitals shown in Figure 4, but the lobes are still oriented in between the coordinated axis. Therefore, the more general label  $t_{2g}$  is more convenient. The orbitals in the  $t_{2g}$  set are no longer completely degenerate. This is probably due to the presence of contributions different from  $d$ -orbitals. This is in agreement with CFT, which reveal that a trigonal distortion splits the  $t_{2g}$  but not the  $e_g$  orbitals in octahedral com-

plexes<sup>83</sup>. For the  $D_{2h}$ -complex, also the degeneracy in the  $e_g$  set is lifted. The reason for this is that the bonds between the ligands and the metal along the  $x$ -axis are compressed, resulting in a stronger repulsion between the  $d_{x^2-y^2}$  orbital and the metal compared to the  $d_{z^2}$  orbital.

The energy difference between the  $e_g$  and  $t_{2g}$  orbital sets,  $\Delta_o$ , can be calculated as the difference between the average energy of the  $e_g$  and  $t_{2g}$  orbitals, being  $9065\text{ cm}^{-1}$  and  $8836\text{ cm}^{-1}$  for the  $S_6$  and  $D_{2h}$  structure respectively. This value is in close agreement with experimental results. Johnson *et al.*<sup>84</sup> obtained a value of  $8400\text{ cm}^{-1}$  starting from experimental absorption spectra via the procedure outlined in Ref.<sup>85</sup>. When comparing this value to the mean pairing energy of  $\text{Co}^{2+}$ ,  $22500\text{ cm}^{-1}$ , we indeed see that the HS state is more stable than the LS state<sup>84,49</sup>.

### 3.3 AOC: $[\text{Co}(\text{H}_2\text{O})_5]^{2+}$

As discussed in Section 2, 5-coordinated complexes can be TBP or SP, with  $D_{3h}$  and  $C_{4v}$  symmetry respectively. For the former, 2 ligands are oriented along the  $z$ -axis and the other ligands lie in the  $xy$ -plane. This configuration can be converted into a SP structure by simple angular distortions as shown by the green arrows in Figure 8. When the angle between the ligand positions 2 and 4 and the metal center is increased until the ligands lie along the  $x$ -axis, they form together with 3 and 5 a square in the  $xz$ -plane indicated with green. As such, the SP structure is obtained, which can easily be recognized after a reorientation of the coordinate axes, indicated with blue arrows in Figure 8. Now, 4 ligands lie in the  $xy$ -plane and the remaining ligand is situated along the  $z$ -axis. The metal center can, but does not have to be in the  $xy$ -plane. It has been observed that most of the 5-coordinated complexes are neither perfectly TBP, nor perfectly SP, but are situated somewhere in between<sup>53</sup>.

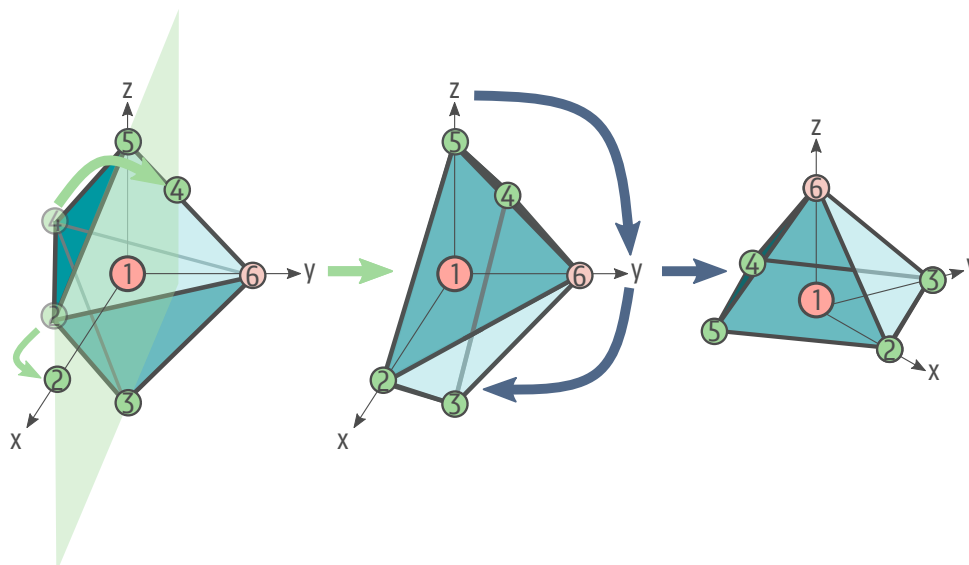


Figure 8: Transformation from a TBP to a SP complex. Ligand positions 2 and 4 are moved until they are situated along the  $x$ -axis and from together with 3 and 5 a square in the  $xz$ -plane indicated in green. This is indicated with green arrows. The SP structures is then obtained after a reorientation of the coordinate axes, indicated with blue arrows.

When the intrinsic structure of the aqua ligands is taken into account, the most symmetric  $[\text{Co}(\text{H}_2\text{O})_5]^{2+}$  complexes have  $C_{2v}$  symmetry, both for the TBP and the SP structures. Optimised geometries have been found with  $C_{2v}$  and  $C_1$  symmetry, for which the latter is slightly more stable (-8600 kJ/mol compared to -8614 kJ/mol). A graphical representation of the symmetry elements and point groups encountered for  $[\text{Co}(\text{H}_2\text{O})_5]^{2+}$  is shown in Figure 9. Structural parameters of the 2 optimised complexes are listed in Table 2.

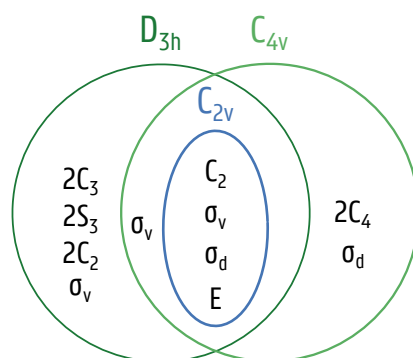


Figure 9: Graphical visualisation of the point groups encountered for the 5-coordinated complexes, *i.e.*,  $D_{3h}$ ,  $C_{4v}$ , and  $C_{2v}$ . All symmetry elements enclosed belong to the corresponding point group.

We performed continuous SHAPE measurements, which evaluate the magnitude of distortion around the metal ion in various complexes<sup>86,87</sup>, in order to determine whether the complexes are closer to the SP or to the TBP symmetry. The resulting continuous shape measures (CShMs) for all 5 possible geometries for 5-coordinated structures are given in Table S4, both for the  $C_{2v}$

and the  $C_1$  complex. From this, we concluded that the  $C_{2v}$  structure is closer to SP, whereas the  $C_1$  structure is closer to TBP. Thus, the TBP complex is a little bit more stable than the SP one. This is in agreement with literature, where it has been shown that the TBP structure is more stable as there is less ligand-ligand repulsion<sup>88</sup>. However, it has been noted that a distorted SP structure may be only slightly less stable<sup>88</sup>.

The splitting of the  $d$ -orbitals along with the atomic contributions is presented in Figure 10, both for the SP and the TBP complex. Again, each MO has a dominant contribution from a specific  $d$ -orbital, which will be used to label the MOs. The orbitals are shown in Figures S3 and S4. In general, the results are in agreement with the theoretical predictions shown in Figure 3, but some differences should be mentioned. The gap between the  $d_{x^2-y^2}$  and  $d_{z^2}$  orbitals is rather large for the SP complex. Furthermore,  $d_{xz}$  and  $d_{yz}$  are not completely degenerate. This is not surprising since the complex only has  $C_{2v}$  symmetry and not  $C_{4v}$ , for which the results are shown in Figure 3. The degeneracy is also lifted for the TBP complex as  $d_{xz}/d_{yz}$  and  $d_{x^2-y^2}/d_{xy}$  are no longer degenerate.

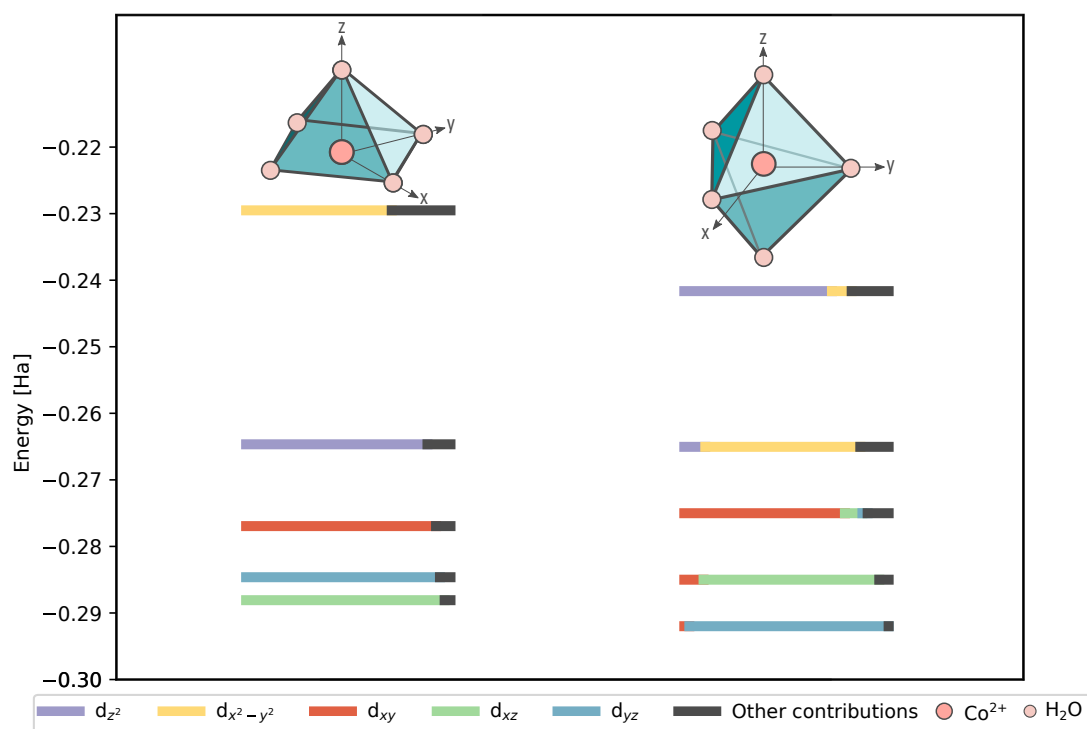


Figure 10: Splitting of the  $d$ -orbitals along with their atomic contributions for the optimised  $[Co(H_2O)_5]^{2+}$  complexes with  $C_{2v}$  symmetry (left pane) and no symmetry (right pane).

### 3.4 AOC: $[\text{Co}(\text{H}_2\text{O})_4]^{2+}$

When another ligand is removed,  $[\text{Co}(\text{H}_2\text{O})_4]^{2+}$  complexes are obtained, in which the aqua ligands are situated at the corners of a tetrahedron. When the intrinsic structure of the aqua ligands is taken into account, the most symmetric complexes have  $D_{2d}$  symmetry, unlike the  $T_d$  symmetry which is found for point-like ligands. In our calculations, the optimised structure does not possess any symmetry. The symmetry elements and point groups encountered for  $[\text{Co}(\text{H}_2\text{O})_4]^{2+}$  are represented graphically in Figure 11. Structural parameters are listed in Table S5.

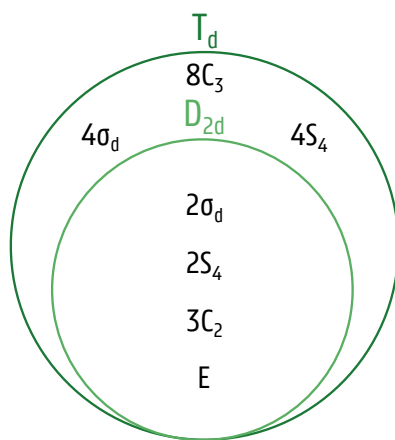


Figure 11: Graphical visualisation of the point groups encountered for the 4-coordinated complexes, *i.e.*,  $T_d$  and  $D_{2d}$ . All symmetry elements enclosed belong to the corresponding point group.

The splitting of the  $d$ -orbitals and the atomic contributions are shown in Figure 12 and the orbitals are presented in Figure S5. The results are in good agreement with those obtained in Figure 3: 2 orbital sets can be distinguished,  $t_{2g}$  and  $e_g$ , where the former is less stable than the latter. Due to the fact that the complex is not purely tetrahedral, the degeneracy in the  $t_{2g}$  set is lifted slightly. Furthermore, the computed value of  $\Delta_t$  is  $5161 \text{ cm}^{-1}$ , which is much smaller than  $\Delta_o$ , as we expected from AOM.

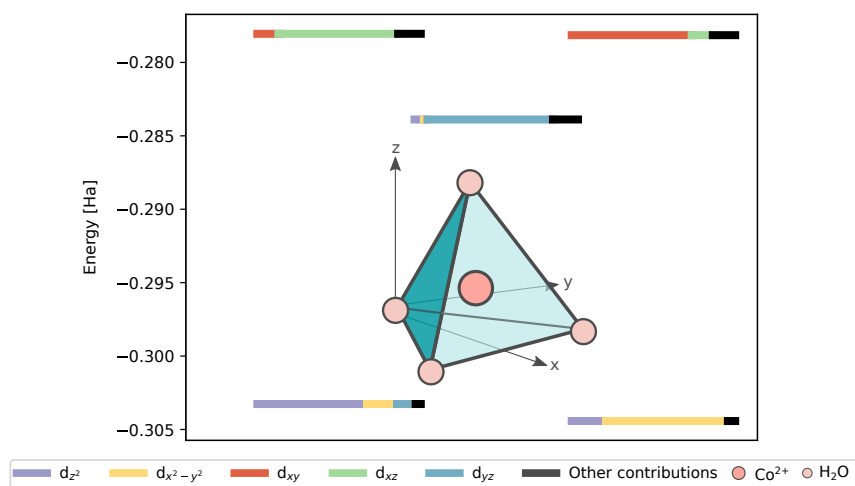


Figure 12: Splitting of the  $d$ -orbitals along with their atomic contributions for the optimised  $[\text{Co}(\text{H}_2\text{O})_4]^{2+}$  complex.

### 3.5 Comparison of AOC with UDFT

We compared the AOC results with these from UDFT calculations. The  $\beta$   $d$ -orbital energy levels along with their atomic contributions are shown in Figure 13 for  $[\text{Co}(\text{H}_2\text{O})_6]^{2+}$ , as calculated with UDFT. The orbitals are presented in Figure S6 and S7 for completeness. Some major distinctions compared to the AOC results need to be highlighted. First of all, remark that the splitting of the  $d$ -orbitals, 50288 and 53232  $\text{cm}^{-1}$  for  $S_6$  and  $D_{2h}$  respectively, is one order of magnitude larger than for the AOC results and the experimentally found splitting presented in Section 3.2. Secondly, the  $t_{2g}$  set is divided into 2 low-lying orbitals and one orbital, which is higher in energy. The reason for this is that only 2 of the  $\beta$   $d$ -orbitals are occupied, resulting in a gap between the highest occupied MO (HOMO) and the lowest unoccupied MO (LUMO).

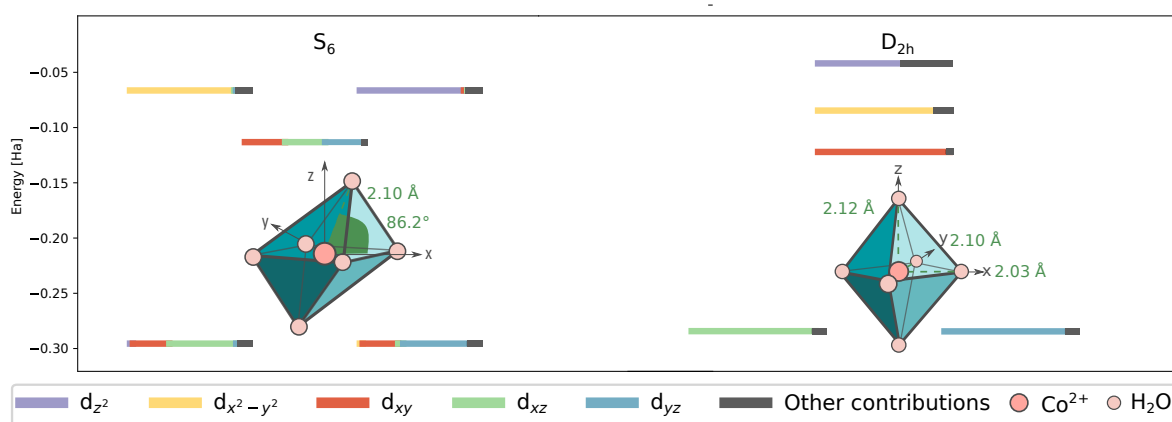


Figure 13: Splitting of the  $d$ -orbitals for the optimised  $[\text{Co}(\text{H}_2\text{O})_6]^{2+}$  complexes with  $S_6$  (left pane) and  $D_{2h}$  (right pane) symmetry calculated by UDFT. Some bond lengths [ $\text{\AA}$ ] and bond angles [ $^\circ$ ] are also indicated.

Additionally, in the UDFT results of the  $D_{2h}$  complex,  $d_{z^2}$  is higher in energy than  $d_{x^2-y^2}$ , as compared to the AOC results. A possible explanation for this observation could be that UDFT and LFT treat the interelectron repulsion differently, as argued by Deeth *et al.* for square planar  $d^8$  Pd-complexes<sup>89</sup>. The interelectron repulsion effects are included within a central field approximation in LFT, whereas in UDFT no central field is assumed and the calculations are performed using the true molecular symmetry of the complex<sup>89</sup>. Therefore, on the one hand, the LFT predictions are in agreement with the AOC results, in which approximate spherical states are constructed by imposing equal fractional occupations. On the other hand, as in the UDFT approach only  $d_{yz}$  and  $d_{xz}$  are occupied, there is more interelectron repulsion along the  $z$ -axis than along the  $x$ - or  $y$ -axis. Therefore,  $d_{z^2}$  will be higher in energy than  $d_{x^2-y^2}$ . Inspired by the work of Deeth *et al.*, we verified this by systematically removing some portion of the electrons from  $d_{xz}$  and  $d_{yz}$  and placing it on  $d_{xy}$ . Therefore, single point UDFT calculations in which the occupation of the  $d$ -orbitals is specified, are performed. The results are shown in Figure 14. Two observations can be made as more and more of the electrons initially on  $d_{xz}$  and  $d_{yz}$  are transferred to  $d_{xy}$ . First of all, the orbitals become closer in energy and are almost degenerate when 0.66 of an electron is placed at  $d_{xy}$ . The reason for this is that the 2  $\beta$  electrons are now almost equally divided among the three orbitals, resulting in a similar interelectron repulsion along the  $x$ -,  $y$ -, and  $z$ -axes. Secondly, as more of the electrons is transferred,  $d_{z^2}$  and  $d_{x^2-y^2}$  increase and decrease in energy, respectively. At an occupation of 0.6 electrons for  $d_{xy}$ , the two most energetic orbitals presented in Figure 14 have similar contributions of  $d_{z^2}$  and  $d_{x^2-y^2}$  and are almost degenerate. When  $d_{xy}$  is populated even more,  $d_{x^2-y^2}$  becomes higher in energy than  $d_{z^2}$ .

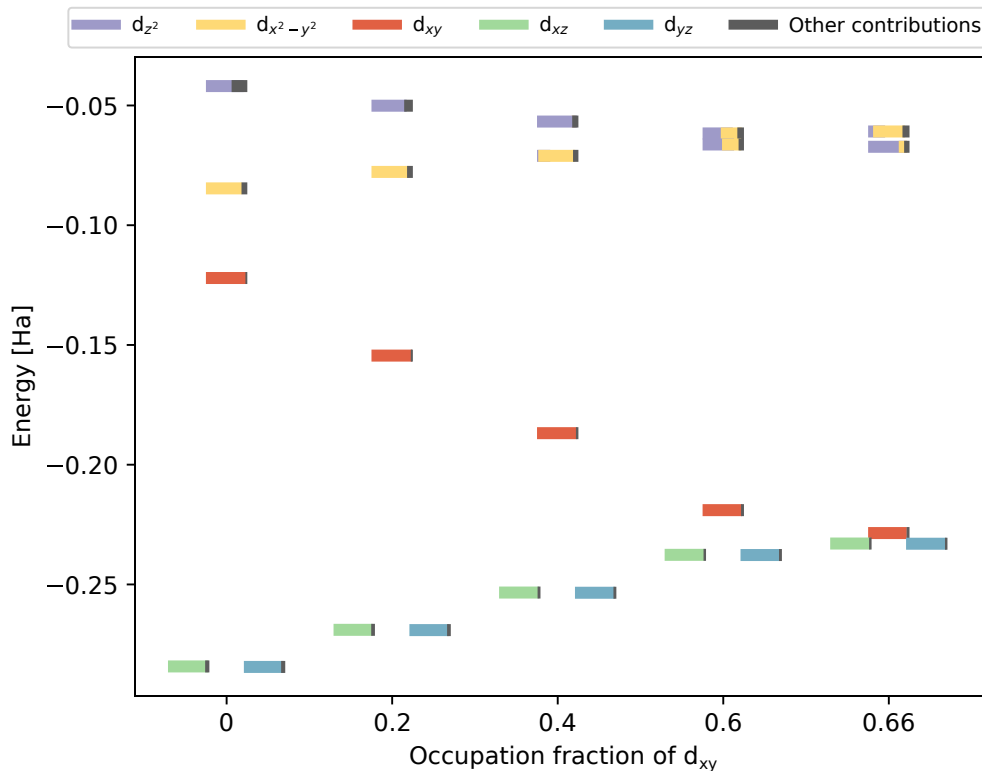


Figure 14: Variation of the splitting of the  $d$ -orbitals as a function of the electron occupation fraction of  $d_{xy}$  which is transferred equally from  $d_{xz}$  and  $d_{yz}$  for the  $[\text{Co}(\text{H}_2\text{O})_6]^{2+}$  complex with  $D_{2h}$  symmetry.

In the UDFT results for the  $S_6$  complex, the  $d_{x^2-y^2}$  and  $d_{z^2}$  orbitals are degenerate just like in the AOC results. Indeed, the effect of the difference in interelectron repulsion is smaller as the two occupied  $d$ -orbitals do not only have contributions from  $d_{yz}$  and  $d_{xz}$ , but also from  $d_{xy}$ . This is shown in Figure S8. As the population of the initially non-occupied orbital increases, the orbitals with contributions from  $d_{xy}$ ,  $d_{xz}$ , and  $d_{yz}$  become more and more degenerate. However, the energy and contribution of the  $d_{x^2-y^2}$  and  $d_{z^2}$  orbitals remain similar.

Deviations from the theoretically predicted  $d$ -orbital splittings are also observed in the 5-coordinated complexes as shown in Figure S9. For both SP and TBP, the energy splitting is one order of magnitude larger compared to the AOC calculations. Furthermore, in the SP complex,  $d_{x^2-y^2}$  and  $d_{z^2}$  are interchanged and are almost degenerate. Again, this is probably due to the different treatment of interelectron repulsion in LFT and UDFT. In the latter, only  $d_{xz}$  and  $d_{yz}$  are occupied, resulting in more interelectron repulsion along the  $z$ -axis, and therefore  $d_{z^2}$  being higher in energy than  $d_{x^2-y^2}$ . Figure S10 justifies this statement: when  $d_{xy}$  is occupied by more than 0.2 electron,  $d_{x^2-y^2}$  is higher in energy than  $d_{z^2}$ . The order of  $d_{z^2}$  and  $d_{x^2-y^2}$  in the TBP complex is in accordance with the AOC results. Just like for the  $[\text{Co}(\text{H}_2\text{O})_6]^{2+}$  complex with  $S_6$  symmetry,

this is due to the mixed  $d$ -orbital contributions of the two lowest occupied MOs. Figure S11 indeed reveals that the orbital energies of the  $d_{z^2}$  and  $d_{x^2-y^2}$  vary only slightly with the orbital population of  $d_{xy}$ .

For the 4-coordinated complexes, presented in Figure S12, the 2 lowest  $\beta$   $e$ -orbitals are occupied, and therefore, the splitting is in accordance with the AOC and theoretical results. Nevertheless, the energy gap between the  $e$ - and  $t_2$ -set is still one order of magnitude too large.

As stated in Ref.<sup>89</sup>, the observation that UDFT and AOC result in different  $d$ -orbitals does not necessarily mean that one of these techniques is right whereas the other is wrong. Orbitals themselves are not experimentally observable, and therefore, additional properties need to be calculated, like for example excited states<sup>89</sup>. The excitation of 6-coordinated  $\text{Co}^{2+}$  aqua-complexes have already been the subject of many research<sup>36,37,38,39,40</sup>. However, to the best of our knowledge, similar studies for 5-, and 4-coordinated complexes are not presented yet.

### 3.6 $[\text{V}(\text{H}_2\text{O})_6]^{2+}$ , $[\text{Mn}(\text{H}_2\text{O})_6]^{2+}$ , and $[\text{Ni}(\text{H}_2\text{O})_6]^{2+}$

In order to further test the validity of the UDFT calculations, additional calculations have been performed on  $[\text{V}(\text{H}_2\text{O})_6]^{2+}$ ,  $[\text{Mn}(\text{H}_2\text{O})_6]^{2+}$ , and  $[\text{Ni}(\text{H}_2\text{O})_6]^{2+}$ , having 3, 5, and 8  $d$ -electrons respectively. These transition metals have been selected as the  $t_{2g}$  set is now completely filled with  $\alpha$  electrons for  $\text{V}^{2+}$  and  $\text{Mn}^{2+}$  or  $\beta$  electrons for  $\text{Ni}^{2+}$ . This is in contrast to the partially filled  $t_{2g}$  set in  $[\text{Co}(\text{H}_2\text{O})_6]^{2+}$  containing 2  $\beta$  electrons. As such, no JT effects are expected for these systems since the  $e_g$  and  $t_{2g}$  sets are each evenly occupied. This is also observed from the calculations for the  $\text{V}^{2+}$  and  $\text{Ni}^{2+}$  complexes as stable complexes with  $T_h$  symmetry are retrieved. However, this is not the case for the  $\text{Mn}^{2+}$  complex, for which the most symmetric stable complexes have  $S_6$  and  $D_{2h}$  symmetry. Systems with  $S_6$  and  $D_{2h}$  symmetry have also been obtained for  $\text{V}^{2+}$  and  $\text{Ni}^{2+}$ . All structures have, within 3 kJ/mol, the same energy and we will show and discuss the results for the complexes with  $S_6$  symmetry. The  $d$ -orbital splittings along with the atomic contributions are shown in Figures 15, S13, and S14 for  $[\text{Mn}(\text{H}_2\text{O})_6]^{2+}$ ,  $[\text{V}(\text{H}_2\text{O})_6]^{2+}$ , and  $[\text{Ni}(\text{H}_2\text{O})_6]^{2+}$  respectively. For  $\text{Mn}^{2+}$  and  $\text{V}^{2+}$  the  $\alpha$ -electrons are shown for the UDFT calculations, whereas the  $\beta$ -electrons are presented for  $\text{Ni}^{2+}$ . The reason for this is that the spin-allowed  $d-d$  transitions will be within  $\alpha/\beta$ -electrons for  $\text{V}^{2+}/\text{Ni}^{2+}$  respectively. For  $\text{Mn}^{2+}$  there are no spin-allowed  $d-d$  transitions. Firstly, remark that, for all the systems,

both AOC and UDFT correctly predict the splitting into a  $t_{2g}$  and  $e_g$  set, which is in agreement with the qualitative LFT results. This is due to the fact that for these systems, the  $t_{2g}$  orbitals are, either completely filled with  $\alpha$ -electrons, as is the case for  $\text{Mn}^{2+}$  and  $\text{V}^{2+}$ , or with both  $\alpha$ - and  $\beta$ -electrons, as is the case for the  $\text{Ni}^{2+}$  complex. Secondly, for  $[\text{Mn}(\text{H}_2\text{O})_6]^{2+}$ , all  $\alpha$ - $d$ -orbitals are occupied, which results in a correct prediction of the magnitude of the  $d$ -orbital splitting by both AOC and UDFT. This result is not surprising since the only differences between the AOC and UDFT calculations are due to the spin polarization which is absent in the former. However, as is the case for the  $\text{Co}^{2+}$  complex, the splitting is severely overestimated by UDFT for  $[\text{V}(\text{H}_2\text{O})_6]^{2+}$  and  $[\text{Ni}(\text{H}_2\text{O})_6]^{2+}$ . This is also shown in Table 2 in which the  $d$ -orbital splitting obtained from experiment<sup>49</sup>, AOC, and UDFT calculations is presented for the various complexes. This observation is in agreement with Ref.<sup>89</sup>, in which it was argued that DFT is expected to yield the same  $d$ -orbitals sequence as LFT in those cases where a suitable spherical configuration is constructed corresponding to equal populations of the  $d$ -orbitals as for  $d^{10}$  or HS  $d^5$  complexes. Here, this observation is confirmed and extended to octahedral  $d^3$ ,  $d^5$ , and  $d^8$  systems.

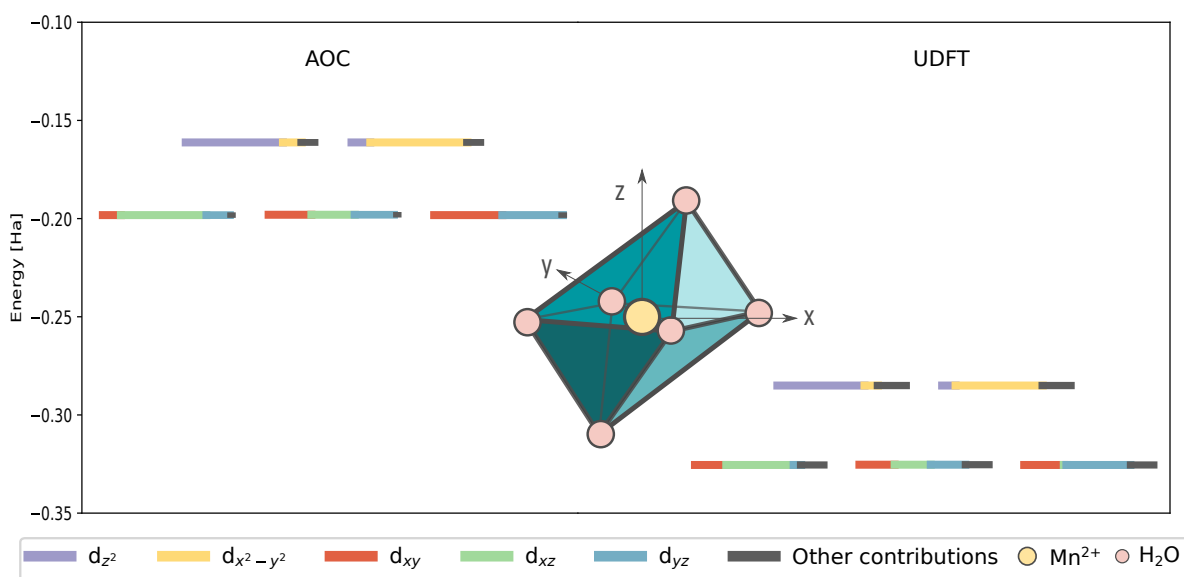


Figure 15: Splitting of the  $d$ -orbitals for the optimised  $[\text{Mn}(\text{H}_2\text{O})_6]^{2+}$  complexes with  $S_6$  symmetry using AOC (left pane) and UDFT (right pane)

	$[\text{V}(\text{H}_2\text{O})_6]^{2+}$	$[\text{Mn}(\text{H}_2\text{O})_6]^{2+}$	$[\text{Ni}(\text{H}_2\text{O})_6]^{2+}$
AOC	11883	8104	10092
UDFT	43359	8868	52155
Experiment <sup>49</sup>	12300	7850 <sup>a</sup>	8600

Table 2:  $d$ -orbital splitting of  $[\text{V}(\text{H}_2\text{O})_6]^{2+}$ ,  $[\text{Mn}(\text{H}_2\text{O})_6]^{2+}$ , and  $[\text{Ni}(\text{H}_2\text{O})_6]^{2+}$  calculated using AOC and UDFT. The experimental value is also included. <sup>a</sup> Estimated value.

## 4 Conclusions

In this work, we investigated  $\text{Co}^{2+}$  aqua-complexes with 6, 5, and 4 ligands. The ground state properties have been examined, and a lot of attention has been paid to the electronic structure. More specifically, we focused on the energy splitting of the  $d$ -electrons and how this depends on the symmetry, where both the influence on the coordination environment as well as the specific point group are considered. Qualitative techniques such as CFT and LFT reveal that the  $d$ -orbital splitting is characteristic for the number of ligands coordinated to the TM. In order to obtain quantitative results, DFT calculations have been performed, both AOC and UDFT. Stable  $\text{Co}^{2+}$  aqua-complexes with 6, 5, and 4 ligands have been obtained from UDFT optimizations. We have observed a stable structure containing 6 aqua ligands with  $D_{2h}$  symmetry in which JT distortions are clearly visible. Besides this, we also found a structure with  $S_6$  symmetry. Moreover, we have shown that the AOC method is capable of reproducing the  $d$ -orbital splittings obtained from the qualitative techniques. UDFT calculations do not succeed in this when only part of the  $d$ -orbitals are occupied. Indeed, the energy gap between the  $d$ -orbitals as well as the energy difference between the HOMO and LUMO are overestimated by UDFT for 6-coordinated aqua-complexes. As such, the  $t_{2g}$  orbitals are far from degenerate as we would expect based on qualitative techniques. Based on the work of Deeth *et al.*, we demonstrated that the discrepancies between UDFT and AOC are due to the different treatment of the interelectron repulsion. In order to further test the performance of UDFT, other TMs have been investigated. We selected TMs for which the  $t_{2g}$  set is occupied evenly. The results for these systems are qualitatively in agreement with for example LFT. Furthermore, for  $[\text{Mn}(\text{H}_2\text{O})_6]^{2+}$ , for which all  $\alpha$   $d$ -orbitals are occupied, even the  $d$ -orbital splitting is described correctly and in agreement with the AOC calculations and experimental results. The proper understanding of the electronic structure and symmetry of TMCs is a key element for obtaining insights in the formation process of MOFs and potentially also their defect structures.

## 5 Supporting Information

Extra computational details, visualization of the orbitals, structural information, CShMs for the  $[\text{Co}(\text{H}_2\text{O})_6]^{2+}$  complexes, additional splittings of the  $d$ -orbitals, and geometries of optimized

structures (PDF).

## **6 Acknowledgements**

The authors acknowledge the Research Board of Ghent University (BOF) for funding. The computational resources and services used in this work were provided by VSC (Flemish Supercomputer Center), funded by Ghent University, FWO, and the Flemish Government Department EWI.

## References

- [1] K. S. Park, Z. Ni, A. P. Côté, J. Y. Choi, R. Huang, F. J. Uribe-Romo, H. K. Chae, M. O’Keeffe, and O. M. Yaghi. Exceptional Chemical and Thermal Stability of Zeolitic Imidazolate Frameworks. *Proc. Natl. Acad. Sci. USA*, 103:10186–10191, 2006.
- [2] Z. Öztürk, J. P. Hofmann, M. Lutz, M. Mazaj, N. Z. Logar, and B. M. Weckhuysen. Controlled Synthesis of Phase-Pure Zeolitic Imidazolate Framework Co-ZIF-9. *Eur. J. Inorg. Chem.*, 2015:1625–1630, 2015.
- [3] J. Cravillon, C. A. Schröder, H. Bux, A. Rothkirch, J. Caro, and M. Wiebcke. Formate Modulated Solvothermal Synthesis of ZIF-8 Investigated using Time-Resolved in Situ X-Ray Diffraction and Scanning Electron Microscopy. *CrystEngComm*, 14:492–498, 2012.
- [4] J. Cravillon, R. Nayuk, S. Springer, A. Feldhoff, K. Huber, and M. Wiebcke. Controlling Zeolitic Imidazolate Framework Nano- and Microcrystal Formation: Insight into Crystal Growth by Time-Resolved In Situ Static Light Scattering. *Chem. Mater.*, 23:2130–2141, 2011.
- [5] J. Cravillon, S. Menzer, S.-J. Lohmeier, A. Feldhoff, K. Huber, and M. Wiebcke. Rapid Room-Temperature Synthesis and Characterization of Nanocrystals of a Prototypical Zeolitic Imidazolate Framework. *Chem. Mater.*, 21:1410–1412, 2009.
- [6] J. Cravillon, C. A. Schröder, R. Nayuk, J. Gummel, K. Huber, and M. Wiebcke. Fast Nucleation and Growth of ZIF-8 Nanocrystals Monitored by Time-Resolved In Situ Small-Angle and Wide-Angle X-Ray Scattering. *Angew. Chem.*, 123:8217–8221, 2011.
- [7] S. R. Venna, J. B. Jasinski, and M. A. Carreon. Structural Evolution of Zeolitic Imidazolate Framework-8. *J. Am. Chem. Soc.*, 132:18030–18033, 2010.
- [8] A. Phan, C. J. Doonan, F. J. Uribe-Romo, C. B. Knobler, M. O’Keeffe, and O. M. Yaghi. Synthesis, Structure, and Carbon Dioxide Capture Properties of Zeolitic Imidazolate Frameworks. *Acc. Chem. Res.*, 43:58–67, 2010.
- [9] H. Hayashi, A. P. Côté, H. Furukawa, M. O’Keeffe, and O. M. Yaghi. Zeolite A Imidazolate Frameworks. *Nat. Mater.*, 6:501–506, 2007.
- [10] C. Fedorchuk and T. W. Swaddle. Comment on Reinterpretation of the Spectra of Hydrated  $\text{Co}^{++}$ : An ab Initio Study (J. Phys. Chem. A 1998, 102, 6525). *J. Phys. Chem. A*, 104:5651–5652, 2000.

- [11] J. Yao and H. Wang. Zeolitic Imidazolate Framework Composite Membranes and Thin Films: Synthesis and Applications. *Chem. Soc. Rev.*, 43:4470–4493, 2014.
- [12] Y. Sun, S. M. J. Rogge, A. Lamaire, S. Vandenbrande, J. Wieme, C. R. Siviour, V. Van Speybroeck, and J.-C. Tan. High-Rate Nanofluidic Energy Absorption in Porous Zeolitic Frameworks. *Nat. Mater.*, 20:1015–1023, 2021.
- [13] Y. Hu, H. Kazemian, S. Rohani, Y. Huang, and Y. Song. In Situ High Pressure Study of ZIF-8 by FTIR Spectroscopy. *Chem. Commun.*, 47:12694–12696, 2011.
- [14] C.-Y. Sun, C. Qin, X.-L. Wang, G.-S. Yang, K.-Z. Shao, Y.-Q. Lan, Z.-M. Su, P. Huang, C.-G. Wang, and E.-B. Wang. Zeolitic Imidazolate Framework-8 as Efficient pH-Sensitive Drug Delivery Vehicle. *Dalton Trans.*, 41:6906–6909, 2012.
- [15] S. A. Moggach, T. D. Bennett, and A. K. Cheetham. The Effect of Pressure on ZIF-8: Increasing Pore Size with Pressure and the Formation of a High-Pressure Phase at 1.47GPa. *Angew. Chem. Int. Ed.*, 48:7087–7089, 2009.
- [16] G. Kaur, R. K. Rai, D. Tyagi, X. Yao, P.-Z. Li, X.-C. Yang, Y. Zhao, Q. Xu, and S. K. Singh. Room-Temperature Synthesis of Bimetallic CoZn Based Zeolitic Imidazolate Frameworks in Water for Enhanced CO<sub>2</sub> and H<sub>2</sub> Uptakes. *J. Mater. Chem. A*, 4:14932–14938, 2016.
- [17] H. T. Kwon, H.-K. Jeong, A. S. Lee, H. S. An, and J. S. Lee. Heteroepitaxially Grown Zeolitic Imidazolate Framework Membranes with Unprecedented Propylene/Propane Separation Performances. *J. Am. Chem. Soc.*, 137:12304–12311, 2015.
- [18] C. Wang, F. Yang, L. Sheng, J. Yu, K. Yao, L. Zhang, and Y. Pan. Synthesis of Isoalkanes over a Core (FeZnZr)Shell (Zeolite) Catalyst by CO<sub>2</sub> Hydrogenation. *Chem. Commun.*, 52:12578–12581, 2016.
- [19] H. Yang, X.-W. He, F. Wang, Y. Kang, and J. Zhang. Doping Copper into ZIF-67 for Enhancing Gas Uptake Capacity and Visible-Light-Driven Photocatalytic Degradation of Organic Dye. *J. Mater. Chem.*, 22:21849–21851, 2012.
- [20] Y.-R. Lee, M.-S. Jang, H.-Y. Cho, H.-J. Kwon, S. Kim, and W.-S. Ahn. ZIF-8: A Comparison of Synthesis Methods. *Chem. Eng. J.*, 271:276–280, 2015.
- [21] R. Banerjee, A. Phan, B. Wang, C. Knobler, H. Furkawa, M. O’Keeffe, and O. M. Yaghi.

- High-Throughput Synthesis of Zeolitic Imidazolate Frameworks and Application to CO<sub>2</sub> Capture. *Science*, 319:939–943, 2008.
- [22] M. J. Van Vleet, T. Weng, X. Li, and J. R. Schmidt. In Situ, Time-Resolved, and Mechanistic Studies of Metal-Organic Framework Nucleation and Growth. *Chem. Rev.*, 118:3681–3721, 2018.
- [23] J. D. Rimer and M. Tsapatsis. Nucleation of Open Framework Materials: Navigating the Voids. *MRS Bull.*, 41:393–398, 2016.
- [24] M. Filez, C. Caratelli, M. Rivera-Torrente, F. Muniz-Miranda, M. Hoek, M. Altelaar, A. J. R. Heck, V. Van Speybroeck, and B. M. Weckhuysen. Elucidation of the Pre-Nucleation Phase Directing Metal-Organic Framework Formation. *Cell Rep. Phys. Sc.*, 2:100680, 2021.
- [25] V. Barone, S. Alessandrini, M. Biczysko, J. R. Cheeseman, D. C. Clary, A. B. McCoy, R. J. DiRisio, F. Neese, M. Melosso, and C. Puzzarini. Computational Molecular Spectroscopy. *Nat. Rev. Methods Primers*, 1, 2021.
- [26] S. Stepanovic, M. Zlatar, M. Swart, and M. Gruden. The Irony of Manganocene: An Interplay between the JahnTeller Effect and Close-Lying Electronic and Spin States. *J. Chem. Inf. Model.*, 59:1806–1810, 2019.
- [27] B. M. Flöser, Y. Guo, C. Riplinger, F. Tuczek, and F. Neese. Detailed Pair Natural Orbital-Based Coupled Cluster Studies of Spin Crossover Energetics. *J. Chem. Theory Comput.*, 16:2224–2235, 2020.
- [28] V. Stavila, I. Bulimestru, A. Gulea, A. C. Colson, and K. H. Whitmire. Hexaaquacobalt(II) and Hexaaquanickel(II) bis( $\mu$ -pyridine-2,6-dicarboxylato)bis[(pyridine-2,6-dicarboxyl-ato)bismuthate(III)] dihydrate. *Acta Cryst. Sect. C: Cryst. Struct. Commun.*, 67:m65–m68, 2011.
- [29] C. K. Jørgensen. Studies of Absorption Spectra. IV. Some New Transition Group BANDs of Low Intensity. *Acta Chem. Scand.*, 8:1502–1512, 1954.
- [30] O. G. Holmes and D. S. McClure. Optical Spectra of Hydrated Ions of the Transition Metals. *J. Chem. Phys.*, 26:1686, 1957.
- [31] C. K. Jørgensen. *Spectroscopy of Transition-Group Complexes in Advances in Chemical Physics*. John Wiley and Sons, Inc., 1963.

- [32] C. K. Jørgensen. *Absorption Spectra and Chemical Bonding in Complexes*. Pergamon Press, 1962.
- [33] J. S. Griffith. *The Theory of Transition-Metal Ions*,. Cambridge University press, 1964.
- [34] R. Spezia, G. Tournois, J. Tortajada, T. Cartailier, and M.-P. Gaigeot. Toward a DFT-Based Molecular Dynamics Description of Co(II) Binding in Sulfur-Rich Peptide. *Phys. Chem. Chem. Phys.*, 8:2040–2050, 2006.
- [35] P. R. Varadwaj and H. M. Marques. The Physical Chemistry of Coordinated Aqua-, Ammine-, and Mixed-Ligand  $\text{Co}^{2+}$  Complexes: DFT Studies on the Structure, Energetics, and Topological Properties of the Electron Density. *Phys. Chem. Chem. Phys.*, 12:2126–2138, 2010.
- [36] F. Neese, T. Petrenko, D. Ganyushin, and G. Olbrich. Advanced Aspects of Ab Initio Theoretical Optical Spectroscopy of Transition Metal Complexes: Multiplets, Spin-Orbit Coupling and Resonance Raman Intensities. *Coord. Chem. Rev.*, 251:288–327, 2007.
- [37] J. C. A. Boeyens and J. F. Ogilvie. *Models, Mysteries and Magic of Molecules*. Springer, 2008.
- [38] Y. Yang, M. A. Ratner, and G. C. Schatz. Multireference Ab Initio Study of Ligand Field dd Transitions in Octahedral Transition-Metal Oxide Clusters. *J. Phys. Chem. C*, 118:29196–29208, 2014.
- [39] F. Vlahovic, M. Peric, M. Gruden-Pavlović, and M. Zlatar. Assessment of TD-DFT and LF-DFT for Study of d-d Transitions in First Row Transition Metal Hexaaqua Complexes. *J. Chem. Phys.*, 142, 2015.
- [40] M. Radon and G. Drabik. Spin states and other ligand-field states of aqua complexes revisited with multireference ab initio calculations including solvation effects. *J. Chem. Theor. Comput.*, 14:4010–4027, 2018.
- [41] H. Bethe. Termaufspaltung in Kristallen. *Ann. Phys.*, 3:133–208, 1929.
- [42] J. H. Van Vleck. Theory of the Variations in Paramagnetic Anisotropy Among Different Salts of the Iron Group. *Physical Review*, 41:208–215, 1932.
- [43] J. H. Van Vleck. Valence Strength and the Magnetism of Complex Salts. *J. Chem. Phys.*, 3:807–813, 1935.

- [44] J. S. Griffith and L. E. Orgel. Ligand-Field Theory. *Q. Rev. Chem. Soc.*, 11:381–393, 1957.
- [45] E. Larsen and G. N. La Mar. The Angular Overlap Model: How to use it and why. *J. Chem. Educ.*, 51:633–640, 1974.
- [46] J. K. Burdett. *Molecular Shapes*. J. Wiley, 1980.
- [47] M. Atanasov, C. A. Daul, and C. Rauzy. A DFT Based Ligand Field Theory. *Struct Bond.*, 106:97–125, 2004.
- [48] M. Ciampolini. *Spectra of 3d Five-Coordinate Complexes*. Springer, 1969.
- [49] G. L. Miessler, P. J. Fischer, and D. A. Tarr. *Inorganic Chemistry*. Pearson, 2014.
- [50] E. I. Solomon, E. G. Pavel, K. E. Loeb, and C. Campochiaro. Magnetic Circular Dichroism Spectroscopy as a Probe of the Geometric and Electronic Structure of Non-Heine Ferrous Enzymes. *Coord. Chem. Rev.*, 114:369–460, 1995.
- [51] D. F. Schriver, P. W. Atkins, and C. H. Langford. *Inorganic Chemistry*. H. Freeman and Co, 1994.
- [52] A. M. Schmiedekamp, M. D. Ryan, and R. J. Deeth. Six-Coordinate  $\text{Co}^{2+}$  with  $\text{H}_2\text{O}$  and  $\text{NH}_3$  Ligands: Which Spin State Is More Stable? *Inorg. Chem.*, 41:5733–5743, 2002.
- [53] L. Sacconi. Five-Coordination in 3d Complexes. *Pure and Applied Chemistry*, 17:95–128, 1968.
- [54] L. Sacconi. Some Factors Governing the Spin-Multiplicity of 5-Coordinate Complexes of Cobalt(II) and Nickel(II). *J. Chem. Soc. (A)*, :248–256, 1970.
- [55] J. C. Slater. *The Self-consistent Field for Molecules and Solids*. McGraw-Hill, New York, 1974.
- [56] G. te Velde, F. M. Bickelhaupt, E.J. Baerends, C. Fonseca Guerra, S.J.A. van Gisbergen, J.G. Snijders, and T. Ziegler. Chemistry with ADF. *J. Comp. Chem.*, 22:931–967, 2001.
- [57] C. C. Pye and T. Ziegler. An Implementation of the Conductor-Like Screening Model of Solvation Within the Amsterdam Density Functional Package. *Theor. Chem. Acc.*, 101:396–408, 1999.
- [58] E. van Lenthe, E. J. Baerends, and J. G. Snijders. Relativistic Regular Two-Component Hamiltonians. *J. Chem. Phys.*, 99:4597, 1993.

- [59] E. van Lenthe, E. J. Baerends, and J. G. Snijders. Relativistic total energy using regular approximations. *J. Chem. Phys.*, 101:9783–9792, 1994.
- [60] E. van Lenthe, A. Ehlers, and E. J. Baerends. Geometry Optimization in the Zero Order Regular Approximation for Relativistic Effects. *J. Chem. Phys.*, 110:8943–8953, 1999.
- [61] S. Grimme, J. Antony, S. Ehrlich, and H. Krieg. A Consistent and Accurate Ab Initio Parametrization of Density Functional Dispersion Correction (DFT-D) for the 94 Elements H-Pu. *J. Chem. Phys.*, 132:154104, 2010.
- [62] C. Lee, W. Yang, and R. G. Parr. Development of the Colle-Salvetti Correlation-Energy Formula into a Functional of the Electron Density. *Phys. Rev. B*, 37:785, 1988.
- [63] A. D. Becke. Density-functional exchange-energy approximation with correct asymptotic behavior. *Phys. Rev. A*, 38:3098–3100, 1988.
- [64] Y. Zhao and D. G. Truhlar. A New Local Density Functional for Main-Group Thermochemistry, Transition Metal Bonding, Thermochemical Kinetics, and Noncovalent Interactions. *J. Chem. Phys.*, 125:194101:1–18, 2006.
- [65] H. S. Yu, X. He, and D. G. Truhlar. MN15-L: A New Local Exchange-Correlation Functional for Kohn-Sham Density Functional Theory with Broad Accuracy for Atoms, Molecules, and Solids. *J. Chem. Theory Comput.*, 12:1280–1293, 2016.
- [66] A. J. Cohen and N. C. Handy. Dynamic Correlation. *Mol. Phys.*, 99:607–615, 2001.
- [67] A. D. Becke. Density Functional Thermochemistry. III. The Role of Exact Exchange. *J. Chem. Phys.*, 98:5648, 1993.
- [68] X. Xu and W. A. Goddard III. The X3LYP Extended Density Functional for Accurate Descriptions of Nonbond Interactions, Spin States, and Thermochemical Properties. *Proc. Natl. Acad. Sci. USA*, 101:2673–2677, 2004.
- [69] C. Adamo and V. Barone. Toward Reliable Density Functional Methods Without Adjustable Parameters: The PBE0 Model. *J. Chem. Phys.*, 110:6158–6169, 1999.
- [70] H. S. Yu, X. He, S. L. Li, and D. G. Truhlar. MN15: A Kohn-Sham Global-Hybrid Exchange-Correlation Density Functional with Broad Accuracy for Multi-Reference and Single-Reference Systems and Noncovalent Interactions. *Chem. Sci.*, 7:5032–5051, 2016.

- [71] V. N. Staroverov, G. E. Scuseria, J. Tao, and J. P. Perdew. Comparative Assessment of a New Nonempirical Density Functional: Molecules and Hydrogen-Bonded Complexes. *J. Chem. Phys.*, 119:12129–12137, 2003.
- [72] J. Tao, J. P. Perdew, V. N. Staroverov, and G. E. Scuseria. Climbing the Density Functional Ladder: Nonempirical Meta-Generalized Gradient Approximation Designed for Molecules and Solids. *Phys. Rev. Lett.*, 91:146401, 2003.
- [73] T. Yanai, D. P. Tew, and N. C. Handy. A New Hybrid Exchange-Correlation Functional using the Coulomb-Attenuating Method (CAM-B3LYP). *Chem. Phys. Lett.*, 393:51–57, 2004.
- [74] J.-D. Chai and M. Head-Gordon. Long-Range Corrected Hybrid Density Functionals with Damped Atom-Atom Dispersion Corrections. *Phys. Chem. Chem. Phys.*, 10:6615–6620, 2008.
- [75] Roy Dennington, Todd A. Keith, and John M. Millam. Gaussview Version 5, 2019. Semichem Inc. Shawnee Mission KS.
- [76] J. Shee, M. Loipersberger, D. Hait, J. Lee, and M. Head-Gordon. Revealing the Nature of Electron Correlation in Transition Metal Complexes with Symmetry-Breaking and Chemical Intuition. *J. Chem. Phys.*, 154:194109, 2021.
- [77] F. Neese, W. Ames, G. Christian, M. Kampa, D. G. Liakos, D. A. Pantazis, M. Roemelt, P. Surawatanawong, and S. Ye. *Dealing with Complexity in Open-shell Transition Metal Chemistry from a Theoretical Perspective: Reaction Pathways, Bonding, Spectroscopy, and Magnetic Properties in Theoretical and Computational Inorganic Chemistry*. Elsevier Inc., 2010.
- [78] CSD Cambridge UK 2008. Cambridge Structural Database, v. 5.30 (updated to Sept 2009).
- [79] H. A. Jahn and E. Teller. Stability of Polyatomic Molecules in Degenerate Electronic States. I. Orbital Degeneracy. *Proc. R. Soc. London A*, 220-235:161, 1937.
- [80] M. Zlatař, C.-W. Schl pfer, and C. Daul. *A New Method to Describe the Multimode Jahn-Teller Effect Using Density Functional Theory*. Springer, 2009.
- [81] T. K. Kundu, R. Bruyndonckx, C. Daul, and P. T. Manoharan. A density functional approach to the jahn-teller effect of  $[\text{Cu}(\text{en})_3]^{2+}$  as a model for a macrobicyclic cage complex of copper(II). *Inorg. Chem.*, 38:3931–3934, 1999.
- [82] C. Stoll, M. Atanasov, J. Bandemehr, F. Neese, C. Pietzonka, F. Kraus, A. J. Karttunen, and G. Heymann M. Seibald, and H. Huppertz. Coexistence of Two Different Distorted

Octahedral  $[\text{MnF}_6]^{3-}$  Sites in  $\text{K}_3[\text{MnF}_6]$ : Manifestation in Spectroscopy and Magnetism. *Chem. Eur. J.*, 27:9801–9813, 2021.

- [83] B. N. Figgis and M. A. Hitchman. *Ligand Field Theory and its applications*. Wiley, 2000.
- [84] D. A. Johnson and P. G. Nelson. Factors Determining the Ligand Field Stabilization Energies of the Hexaaqua  $2+$  Complexes of the First Transition Series and the Irving-Williams Order. *Inorg. Chem.*, 34:5666–5671, 1995.
- [85] J. Reedijk, W. L. Driessen, and W. L. Groeneveld. A Semi-Empirical Energy-Level Diagram for Octahedral Cobalt(II) Complexes. *Recl. Trav. Chim. Pays-Bas Chim*, 88:1095–1109, 1969.
- [86] I. Hargittai. Book Review: Fuzzy Definitions: Concepts in Chemistry A Contemporary Challenge. Edited by D. H. Rouvray. *Angew. Chem. Int. Ed.*, 36:2525–2525, 1997.
- [87] H. Zabrodsky, S. Peleg, and D. Avnir. Continuous Symmetry Measures. *J. Am. Chem. Soc.*, 114:7843–7851, 1992.
- [88] J. Zemann. Elektrostatische Energien von  $\text{AB}_5$ -Komplexen. *Z. Anorg. Allgem. Chem.*, 324:241–249, 1963.
- [89] R. J. Deeth. Ligand Field and Density Functional Descriptions of the d-States and Bonding in Transition Metal Complexes. *Faraday Discuss.*, 124:379–391, 2003.

## Table of Contents synopsis

The influence of the symmetry and number of ligands on the ground state properties, and more specifically the electronic structure, of  $\text{Co}^{2+}$  complexes with 6, 5, and 4 aqua ligands has been studied via computational techniques based on density functional theory. In general, average of configuration calculations are needed to properly describe the characteristic  $d$ -orbital splitting.

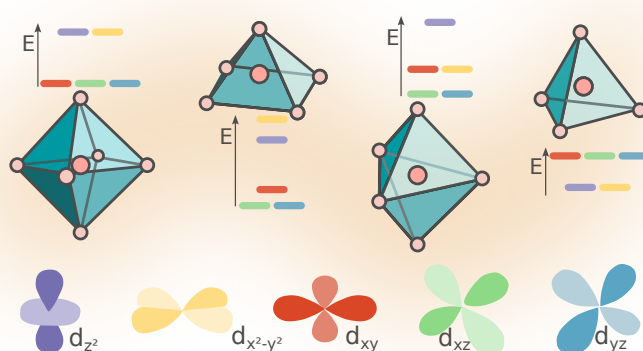


Figure 16: For Table of Contents Only